RSC Advances

ROYAL SOCIETY OF CHEMISTRY

www.rsc.org/advances

Room temperature ferromagnetic $Zn_{0.98}Co_{0.02}O$ powders with improved visible-light photocatalysis

Huiyun Zhang [1], Wei Hao [2], Yanqiang Cao [3], Xiaofeng Chang [4], Mingxiang Xu [1], Xinli Guo [2], Kai Shen [5], Dinghan Xiang [6], and Qingyu Xu [1, 7*]

[1] Department of Physics, Southeast University, Nanjing 211189, & Key Laboratory of MEMS of the Ministry of Education, Southeast University, Nanjing 210096, & Collaborative Innovation Center of Suzhou Nano Science and Technology, Soochow University, Suzhou 215123, China

[2] School of Materials Science and Engineering, Southeast University, Nanjing 211189, China

[3] Department of Materials Science and Engineering, Nanjing University, Nanjing 210008, China

[4] College of Engineering and Applied Sciences, Nanjing University, Nanjing 210093, China

[5] School of Materials Science and Technology, Nanjing University of Aeronautics and Astronautics, Nanjing 210016, China

[6] Guangxi Key Laboratory of Information Materials, Guilin University of Electronic Technology, Guilin 541004, China

[7] National Laboratory of Solid State Microstructures, Nanjing University, Nanjing 210093, China

Abstract:

The realization of ferromagnetic diluted magnetic semiconductors requires the fine tuning of the energy level of band structure, which might have important applications in photocatalysis. The magnetic properties and visible-light photocatalytic properties of $Zn_{0.98}Co_{0.02}O$ nanoparticles post-annealed under different ambient conditions (vaccum, hydrogen, vaccum followed by hydrogen) have been studied. The X-ray diffraction patterns show that all samples have hexagonal wurtzite structure without any impurity phase. However, the Raman spectra indicate the small amount of Co_3O_4 impurities, which is significantly suppressed during the hydrogenation process. The as-prepared and vacuum-annealed $Zn_{0.98}Co_{0.02}O$ nanoparticles show dominant paramagnetic properties, while strong room temperature ferromagnetism is observed after the hydrogenation process. This is explained by the ferromagnetic mediation between doped Co ions by the interstitial H ions. The photocatalytic activity of the resulting samples was evaluated by the degradation of Rhodamine B under visible light irradiation. It was found that the $Zn_{0.98}Co_{0.02}O$ annealed in vacuum exhibited the best photodegradation properties. The enhanced performance is mainly attributed to the existence of oxygen vacancies which might decrease the surface recombination centers and improve the charge separation efficiency. The photocatalysis of hydrogenated sample is deteriorated significantly due to the passivation of oxygen vacancies by hydrogen, which confirms the ferrogmagnetic mediation by H^+ ions instead of oxygen vacancies. Interestingly, the vacuum-annealed $Zn_{0.98}Co_{0.02}O$ samples further annealed under hydrogen ambient condition exhibit both room temperature ferromagnetism and sizable photocatalytic ability.

Key Words: photocatalytic activity, diluted magnetic semiconductors, oxygen vacancy, hydrogenation

*Corresponding author: xuqingyu@seu.edu.cn

Introduction:

Recently, intensive attention has been paid on ZnO-based diluted magnetic semiconductors (DMSs) for their potential applications in spintronics.[1, 2] Among them, room temperature ferromagnetism in Co-doped ZnO DMSs has also been widely studied due to the theoretical predicted and experimental observed high Curie temperature (T_C).[3-7] Some papers reported room temperature ferromagnetism (RTFM) owing to the intrinsic origin of related defects,[6] whereas some other works attributed to the RKKY (or carrier-mediated) character of RTFM.[7] However, Park *et al*.[5] argued that the observed RTFM originated from the nanometer-sized Co clusters. Until now, the origin of RTFM in Co-doped ZnO is still unclear. As an inevitable extrinsic impurity in ZnO, the influence of hydrogen on magnetic properties of Co-doped ZnO DMS systems has further fuelled the research interests. Some groups attributed the reported RTFM to ferromagnetic Co-H-Co exchange interaction by hydrogen mediation,[8, 9] In contrast to this, other studies attributed the RTFM in hydrogenated Co-doped ZnO either to appearance of Co clusters[10] or oxygen vacancies.[11] Thus, the mechanism is still controversial and needs further studies.

Apart from the magnetic study, ZnO has become one of the most researched photocatalysts due to its environmental stability, strong oxidizing power, non-toxicity and long term photostability as compared to other photocatalysts.[12, 13] However, ZnO shows a relatively high electron-hole recombination ratio which is unfavorable for its photocatalytic activity and only responds to UV light because of its wide band gap.[14] Therefore the development of visible light response and inhibiting the recombination of

photogenerated electrons and holes in ZnO is becoming more and more important. Various approaches, such as nonmetals doping,[15, 16] transition metals incorporating,[17, 18] coupling with other metaloxides[19, 20] and combining with carbonaceous materials[21] have been adopted. Among the various methods, incorporation of transition-metal (TM) cations has attracted considerable attention because it may not only introduce magnetic properties but also modify the electronic energy band structure so as to extend its photocatalytic activity to the visible region.[17, 22] However, efficient separation and recovery of the catalyst from treated water hampered the commercial applications of the photocatalysis technology. The usage of magnetically separable photocatalysts is a possible solution. For example, some investigators prepared nanoparticles with magnetic core and photoactive shell,[23, 24] others incorporated ferromagnetic nanoparticles into photocatalysts.[25]

In our previous work,[26] we obtained the RTFM in $Zn_{0.98}Co_{0.02}O$ powders after annealing in H_2 atmosphere. In this paper, post-annealed treatments in various atmosphere (vacuum, H_2, vaccum followed by H_2) were used to modify $Zn_{0.98}Co_{0.02}O$ nanoparticles to clarify the ferromagnetic origin and obtain the ferromagnetic catalyst under visible light. It is found that the oxygen vacancies enhance the photocalytic activities, but suppress the formation of Co–H–Co units, because hydrogen preferentially passivates oxygen vacancy. The ferromagnetic mediation of H^+ between neighboring Co ions has been confirmed. Room temperature ferromagnetic visible light photocatalyst can be obtained by treating $Zn_{0.98}Co_{0.02}O$ nanoparticles with vacuum annealing followed by hydrogenation.

Experimental Details:

$Zn_{0.98}Co_{0.02}O$ nanoparticles were fabricated by sol-gel method. Zinc acetate and cobalt acetate weighted according to the stoichiometry were used as the source materials. Citricacid, ethylene glycol were then dissolved as a complexingagent and stabilizer, respectively. The transparent solution was dried at 120 ^{o}C until the xerogel was generated, then the xerogel was presintered at 300 ^{o}C for 12 h to remove organics. The resulting powders were sintered at 500 ^{o}C for 24 h to obtain the $Zn_{0.98}Co_{0.02}O$ samples. Post thermal treatments (500 ^{o}C for 2 h in vacuum, H_2 and vaccum followed by H_2 atmosphere) were further performed. For convenience, the as-grown sample, vacuum annealed sample, H_2 annealed sample, vacuum followed H_2 annealed sample were denoted as ZnCoO, ZnCoO-Vac, ZnCoO-H, ZnCoO-Vac-H, respectively.

The crystalline structures of the films were examined by X-ray diffraction (XRD) with Cu Kα radiation (1.5406 Å). The particle morphology and size were characterized by a transmission electron microscope (TEM, FEI Tecnai F20). Raman measurements were performed on a Horiba JobinYvonLabRAM HR 800 micro-Raman spectrometer with 514 nm excitation source under air ambient condition at room temperature. The UV-vis diffuse reflectance spectra (DRS) were recorded using a UV-visible spectrophotometer (JASCO, UV-670) with a wavelength range of 200-800 nm. X-ray photoelectron spectroscopy (XPS) was carried out using an X-ray photoelectron spectrometer (ThermoFisher SCIENTIFIC) with Al Kα X-ray source (hν=1486.6 eV). The samples for XPS measurements were kept in the high-vacuum chamber overnight to remove the absorbed air. The magnetic properties were characterized by a physical property measurement system (PPMS, Quantum Design).

The photocatalytic activities of the samples were tested by the photocatalytic decomposition of Rhodamine B (RhB) at room temperature with visible-light irradiation.

Typically, 50 mg of photocatalyst was dispersed in 150 mL of 8 mg L^{-1} RhB aqueous solution. A 500 W Xe lamp (Beijing Trusttech Co Ltd, CHF-XM) equipped with visible pass filter (λ=400-800 nm). The concentrations of model contaminates were monitored at 554 nm by using a UV-vis spectrophotometer (Hitach U-3900).

Results and discussion:

Figure 1 shows the XRD patterns of ZnCoO, ZnCoO-Vac, ZnCoO-H，ZnCoO-Vac-H nanoparticles. It can be seen that all the characteristics peaks match with hexagonal wurtzite structure (space group: $P6_3mc$) without extra peaks. The crystallite size of ZnCoO, ZnCoO-Vac, ZnCoO-H, ZnCoO-Vac-H calculated by Scherrer's formula were tabulated in Tab. 1 using (101) diffraction peak. The results reveal that there is almost no change in the crystallite size of ZnCoO after each annealing process. In Fig. 1(b), it is shown that the diffraction peaks slightly shift towards lower angle after the annealing process. The lattice parameters were listed in Tab. 1, confirming the lattice expansion through the thermal annealing. The microstructure and crystallite size were further investigated by TEM and the image of ZnCoO is shown in Fig. 2. Most nanoparticles are individually more or less spherical in shape and the grain size of ZnCoO is about 33 nm which is consistent with the XRD results. Similar TEM results were obtained for the post-annealed ZnCoO samples.

Figure 3 shows the Raman spectra of as-prepared and post-annealed ZnCoO nanoparticles in the range of 200-800 cm^{-1}. In the forepart of the spectra, all samples have three Raman-active vibration modes at 331, 384, 439 cm^{-1} which are assigned to the typical Raman vibrational modes of the wurtzite phase ZnO.[27, 28] The dominant peak at 439 cm^{-1} for all samples is attributed to E_2 (high) mode. The peak at 331 cm^{-1} is due to the second-order phonon, and the 384 cm^{-1} line is the first-order phonon of A_1(TO).[29] In addition, there is a broad Raman-active vibration mode, among 500–600 cm^{-1} which can

be attributed to the oxygen vacancy.[30] Furthermore, two significant peaks at 528 cm^{-1} and 577 cm^{-1} were observed for ZnCoO-Vac, which suggested the high concentration of oxygen vacancies (V_O). It should be noted that there are three additional modes: 493cm^{-1} is attributed to a surface optical phonon,[31] 629cm^{-1} corresponds to F_{2g} phonon modes of Co_3O_4,[32] and 720 cm^{-1} assigned to the vibration of Co–O bond.[32] Furthermore, a broad peak at 688 cm^{-1} was observed for ZnCoO which corresponds to A_{1g} local vibration mode of Co_3O_4.[33] However, there are no Co_3O_4-related peaks observed in the Raman spectra of ZnCoO-Vac-H and ZnCoO-H, suggesting that hydrogenation process suppresses the formation of Co_3O_4, which is consistent with our previous work.[26]

UV-vis DRS can be used to determine the band gap of semiconductors. Figure 4a shows the UV-vis DRS of ZnO, ZnCoO, ZnCoO-Vac, ZnCoO-H, ZnCoO-Vac-H. Compared with pure ZnO nanoparticles, the absorption edges of as-prepared and post-annealed ZnCoO samples are clearly red-shifted to visible-light region. To further deriving the band-gap energies (E_g), $[F(R)h\nu]^{1/2}$ versus photon energy $h\nu$ is plotted, as shown in Fig. 4b, where F(R) is the Kubelka-Munk function with $F(R) = (1-R)^2/2R$ and $R=R_{sample}/R_{reference}$ equals to the diffuse reflectance in UV-vis spectra.[34] The band energy are determined by extrapolating the linear section of the curves describing the dependence of $[F(R)h\nu]^{1/2}$ on the photon energy $h\nu$ to zero.[35] The linear relation between $[F(R)h\nu]^{1/2}$ and $h\nu$ confirms the direct-band gap in these ZnCoO samples. It is found that the band-gap energy for pure ZnO is 3.11eV, which is lower than the reported value of bulk ZnO (3.37eV).[36] For samples ZnCoO, ZnCoO-Vac, ZnCoO-H, ZnCoO-Vac-H, E_g is 2.58, 2.60, 2.54 and 2.56 eV, respectively. The obviously narrowed band gap of ZnCoO can be interpreted in term of sp–d exchange interactions between the conduction band electrons and the localized d electrons of transition metals ions Co^{2+}.[37] It can be seen that vacuum annealing can slightly increase the band gap of ZnCoO, which can be attributed

to the increase of carrier concentration according to the Burstein–Moss effect.[38] Interestingly, after the hydrogenation, the band gap is slightly decreased, which might be due to the passivation of the Vo by H^+. Another possible explanation is that band gap decreases with increase in particle size,[39] the slightly increase of particles size leads to the decrease of band gap.

To gain more information, XPS spectra were collected to characterize electronic structure of each element. Figure 5 illustrates the typical core level peaks of Co2*p* and O 1*s* XPS spectra, respectively. As show in Fig. 5a, the peak position of Co $2p_{3/2}$ for ZnCoO, ZnCoO-Vac, ZnCoO-H, ZnCoO-Vac-H was 779.7, 780.5, 779.3, 780.4 eV, ruling out the presence of Co metal cluster (peak position should be at 778.0 eV).[40] Moreover the presence of satellite peaks at the higher binding energy can be observed, and the positions are nearly 5-7 eV higher than their main peaks, confirming that the Co ions are mainly bivalent as substituents.[40-43]

The peaks of O 1s shown in Fig. 5b are asymmetric for all the samples, meaning the existence of multiple oxygen species. All the O1*s* peaks can be deconvoluted into two peaks named O_a and O_b by using Gaussian fitting. As shown in Fig. 5b, the O_a peak located around 529.8 eV corresponds to O^{2-} ions surrounded by Zn^{2+}.[44] In terms of higher-binding-energy O_b peak, some reports believe that the peak centering at 531.1 eV is related to oxygen vacancy (Vo).[45, 46] Therefore, the vacancy concentration is denoted by the relative area of the fitting curve. As Fig. 5b shows, the area ratio of the peak O_b to O_a is 0.270, 0.561, 0.339, 0.532 for ZnCoO, ZnCoO-Vac, ZnCoO-H and ZnCoO-Vac-H, respectively. Ren *et al*. suggested that the as-grown samples have plenty of oxygen interstitials (O_i) defects from the growth process, but annealing in hydrogen atmosphere can reduces O_i defects, promotes the formation of Vo.[47] So the ZnCoO samples have the minimum concentration of V_O from the XPS results. Furthermore, Zhang *et al.* believed

that hydrogen can passivate oxygen vacancy.[48] The concentration of Vo in ZnCoO-Vac-H is less than ZnCoO-Vac if the two cases are both existed.

The field dependent magnetization (*M-H*) curves were measured for ZnCoO, ZnCoO-Vac, ZnCoO-H, ZnCoO-Vac-H at 300 K, shown in Fig. 6. Room temperature ferromagnetism was observed both for ZnCoO-H and ZnCoO-Vac-H. ZnCoO-Vac-H has a smaller saturated magnetization value than ZnCoO-H. However, the ZnCoO and ZnCoO-Vac showed nearly linear paramagnetic curves. Only trace amount of Co_3O_4 was observed in ZnCoO and ZnCoO-Vac, and no metallic Co was determined from the XRD and XPS spectra, it can be safely concluded that the ferromagnetic contribution from Co metal cluster can be excluded. Furthermore, from the XPS result, ZnCoO-Vac has the highest concentration of Vo, but only paramagnetism was observed. There is no clear relation between the ferromagnetism and Vo concentration. Thus, the direct ferromagnetic contribution or ferromagnetic mediation between doped Co ions by Vo can be excluded. ZnCoO-H and ZnCoO-Vac-H were treated by hydrogenation under the similar conditions, but the magnetization of ZnCoO-H is larger than that of ZnCoO-Vac-H. This can be understood that the less interstitial H is formed in the presence of larger concentration of Vo because that hydrogen passivation of V_O.[48] The interstitial H^+ ions mediate a strong short-range ferromagnetic exchange interaction between Co^{2+} ions through the formation Co-H-Co,[8] and Vos suppress the mediation of ferromagnetism by trapping the H^+ ions.[49]

The photocatalytic activity of post-annealed ZnCoO materials was conducted by photodegradation of RhB under visible-light irradiation. The contents of RhB molecules were measured from the maximum absorption peak at λ=554 nm of the UV-vis absorption spectra. Figure 7 shows the time dependent photodegradation of RhB in the presence of catalysts. The C/C_0 ratio was utilized to represent the degradation efficiency, where C and C_0 are the RhB concentration at time t and 0, respectively. As shown in Fig.

7, the photocatalytic activity of the sample is ZnCoO-Vac > ZnCoO-Vac-H > ZnCoO > ZnCoO-H, and about 75% of RhB dyemolecules were decomposed within 2 h for ZnCoO-Vac. It is generally accepted, the photogenerated electrons and holes play a major role in photocatalytic reaction. ZnO shows a relatively high electron-hole recombination ratio.[14] If a suitable scavenger or surface defect state is available to trap the electron or hole, recombination is prevented and subsequent redox reactions may occur.[50] Here, the Vos working as electron acceptors are available to trap the photogenerated electrons temporarily to prevent the recombination of electron-hole pairs to further enhance the photocatalystic activity.[51] Moreover, some groups proposed that Vos in ZnO are easily passivated by hydrogen atoms.[48, 52] The phtocatalytic results further confirm that Vo is passivated by H during hydrogenation process which leads to the weaker photocatalytic activity of ZnCoO-H than that of ZnCoO. Due to the much higher concentration of Vo in ZnCoO-Vac, the H^+ ions might only partially passivate the Vos, and still higher concentration of Vos left in ZnCoO-Vac-H after the hydrogenation process. Thus the photocalytic activity of ZnCoO-Vac-H is slightly worse than that of ZnCoO-Vac but still much improved compared with ZnCoO. For ZnCoO-Vac-H, the characteristic absorption band of RhB at 554 nm shown in inset (right) decreased significantly with increasing irradiation time, accompanied by a remarkable blue-shift of the maximum absorption. The step wise blue-shift of the main peak from 554 to 533 nm can be attributed to the step-by-step de-ethylation of RhB.[53] More importantly, the ZnCoO-Vac-H not only exhibits a better photodegradation rate but also room temperature ferromagnetism. After the photocatalytic degradation, ZnCoO-Vac-H can be magnetically recoverable, as shown in inset (left).

Figure 8 displays schematic diagram of the oxygen vacancies-related photocatalytic mechanism. As is generally known, the hydroxyl radical ($\cdot OH^-$) forms either from an

electron via molecular oxygen,[54] or from a hole via adsorbed H_2O on the surface[55] which oxidized the organic pollutants.[54] Here, the band gap does not change significantly with the existence of Vos, and the accompanying Vos can generate isolated states in the forbidden gap.[56] The Vos in ZnCoO samples with unoccupied states can act as potential wells to trap electrons temporarily to reduce the surface recombination of electrons and holes,[51] then the separated electrons combine with molecular oxygen on the surface to generate superoxide anions ($\cdot O^{2-}$) groups, which react with H_2O molecules and finally turn into $\cdot OH^-$ groups.[54] The holes may also adsorb H_2O to form the $\cdot OH^-$ groups to oxidize the organic pollutant.

Conclusions

In summary, the photocatalytic and magnetic characteristics of ZnCoO nanoparticles treated under different ambient are presented. All samples with diameter of about 33 nm have hexagonal wurtzite structure without any secondary phase from XRD patterns. The substitution of cobalt ions in ZnO narrows the band gap to around 2.6 eV, leading the samples to response to visible light irradiation. The concentration of oxygen vacancies is increased by annealing ZnCoO in vacuum ambient, which suppresses the recombination of photogenerated electron-hole pairs and improves the charge separation efficiency to further enhance the photocatalytic activities. The XPS and Raman spectra exclude the presence of Co metal clusters and further indicate that hydrogenation process may suppress the formation of Co_3O_4. The samples annealed in hydrogen atmosphere exhibit room temperature ferromagnetism but deteriorate photocatalytic ability due to the passivation of oxygen vacancy. Our results clearly confirm that the ferromagnetic coupling between doped Co^{2+} ions is mediated by interstitial H^+ ions instead of oxygen vacancies. Furthermore, an efficient ferromagnetic visible light photocatalyst of ZnCoO-Vac-H was successfully fabricated with this separate realization strategy,

enhancing the photocatalytic ability by inducing oxygen vacancies using vacuum annealing and inducing ferromagnetism by ferromagnetic mediation of interstitial H^+.

Acknowledgements

This work is supported by the National Natural Science Foundation of China (51172044, 51471085), the Natural Science Foundation of Jiangsu Province of China (BK20151400 and BK20141337) and Guangxi Key Laboratory of Information Materials (Guilin University of Electronic Technology, Project No: 131007-K).

References

1. Dietl, T.; Ohno, H.; Matsukura, F.; Cibertand, J.; Ferrand, D. Zener Model Description of Ferromagnetism in Zinc-Blende Magnetic Semiconductors. *Science*, 2000, 287, 1019-1022.

2. Lee, H. J.; Jeong, S. Y.; Choan,C. R.; Park, C. H. Study of diluted magnetic semiconductor: Co-doped ZnO. *Appl. Phys. Lett.*, 2002, 81, 4020-4022.

3. Sato, K.; Katayama-Yoshida, H. Material Design for Transparent Ferromagnets with ZnO-Based Magnetic Semiconductors. *Jpn. J. Appl. Phys.*, Part 2, 2000, 39, L555-L558.

4. Ciatto,G.; Trolio, D.; Trolio, A. D.; Fonda, E.; Allippi, P.; Testa, A. M.; Bonapasta, A. A. Evidence of Cobalt-Vacancy Complexes in $Zn_{1-x}Co_xO$ Dilute Magnetic Semiconductors. *Phys. Rev. lett*, 2011,107, 127206.

5. Park, J. H.; Kim, M. G.; Jang, H. M.; SangwooRyu. Co-metal clustering as the origin of ferromagnetism in Co-doped ZnO thin films. *Appl. Phys. Lett.*, 2004, 84, 1338-1340.

6. Wang, X. F.; Xu, J. B.; Ke, N.; Yu, J. G.; Wang, J.; Li, Q.; Ong, H. C.; Zhang, R. Imperfect oriented attachment: Direct activation of high-temperature ferromagnetism in diluted magnetic semiconductor nanocrystals. *Appl. Phys. Lett.*, 2006, 88, 223108.

7. Zhu, T.; Zhan, W. S.; Wang, W. G.; Xiao, J. Q. Room temperature ferromagnetism in two-step-prepared Co-doped ZnO bulks. *Appl. Phys. Lett.*, 2006, 89, 022508.

8. Park, C. H.; Chadi, D. J. Hydrogen-Mediated Spin-Spin Interaction in ZnCoO. *Phys. Rev. lett.*, 2005, 94, 127204.

9. Lee, S.; Cho, Y. C.; Kim, S. –J.; Cho, C. R.; Kim, S. J.; Kim, J. P.; Choi, Y. N.; Sur, J. M.; Jeong, S. –J. Reproducible manipulation of spin ordering in ZnCoO nanocrystals by hydrogen mediation *Appl. Phys. Lett.*, 2009, 94, 212507.

10. Wang, Y.; Sun, L.; Kong, L.; Kang, J.; Zhang, X.; Han, R. Room-temperature ferromagnetism in Co-doped ZnO bulk induced by hydrogenation. *J. Alloys Compd.*, 2006, 423, 256-259.

11. Manivannan, A.; Dutta, P.;Glaspell, G.; Seehra, M. S. Nature of magnetism in Co- and Mn-doped ZnO prepared by sol-gel technique. *J. Appl. Phys.*, 2006, 99, 08M110.

12. Pearton, S. J.; Norton, D. P.; Ip, K.; Heo, Y. W.; Steiner, T. Recent progress in processing and properties of ZnO. *Prog. Mater. Sci*, 2005, 50, 293-340.

13. Mahjoub, A. R.; Movahedi, M.; Kowsari, E.; Yavari, I. Narcis-like zinc oxide: Chiral ionic liquid assisted synthesis, photoluminescence and photocatalytic activity. *Mater. Sci. Semicond. Process.*, 2014, 22, 1-6.

14. F. H. Chu, C. W. Huang, C. L. Hsin, C. W. Wang, S. Y. Yu, P. H. Yeh, W. W. Wu, *Nanoscale*, 2012, 4, 1471-1475.

15. S. B. Sun, X. Chang, X. J. Li, Z. J. Li, *Ceram. Int.*, 2013, 39, 5197-5203.

16. H. S. Yoon, K. S. Lee, T. S. Lee, B. Cheong, D. K. Choi, D. H. Kim, W. M. Kim, *Sol. Energy Mater. Sol. Cells*, 2008, 92, 1366-1372.

17. Y. C. Lu, Y. H. Lin, D. J. Wang, L. L. Wang, T. F. Xie, T. F. Jiang, *Nano Res.*, 2011, 4, 1144–1152.

18. Y. Y. Zhang, M. K. Ram, E. K. Stefanakos, D. Y. Goswami, *Surf. Coat. Technol.*, 2013, 217, 119–123.

19. J. Xie, Z. Zhou, Y. Lian, Y. Hao, X. Liu, M. Li, Y. Wei, *Ceram. Int.*, 2014, 40, 12519–12524.

20. D. Li, H. Haneda, N. Ohashi, S. Hishita, Y. Yoshikawa, *Catal. Today*, 2004, 93, 895–901.

21. X. Chen, Y. He, Q. Zhang, L. Li, D. Hu, T. Yin, *J. Mater. Sci.*, 2010, 45, 953–960.

22. K. Jug, V. A. Tikhomirov, *J. Phys. Chem. A*, 2009, 113, 11651–11655.

23. W. Yan, H. P. Fan, C. Yang, *Mater. Lett*, 2011, 651, 1595–1597.

24. F. Chen, Y. D. Xie, J. C. Zhao, G. X. Lu, *Chemosphere*, 2001, 44, 1159–1168.

25. H. Pang, Y. C. Li, L. N. Guan, Q. Y. Lu and F. Gao, *Catal. Commun.*, 2011, 12, 611-615.

26. H. Zhang, Y. Q. Cao, Z. X. Yang, L. F. Si, W. Zhong, D. Wu, M. X. Xu, Q. Y. Xu, *Mater. Lett*, 2012, 89, 209–211.

27. R. Y. Sato-Berru, A. Vázquez-Olmos, A. L. Fernández-Osorio and S. Sotres-Martínez, *J. Raman Spectrosc.*, 2007, 38, 1073–1076.

28. R. Cusco´, E. Alarco´n-Llado´, J. Iba´n˜ez, L. Artu´s, J. Jime´nez, B. Wang, M. J. Callahan, *Phys. Rev. B*, 2007, 75, 165202

29. H. Harima, *J. Phys.:Condens. Matter*, 2004, 16, S5653.

30. C. J. Youn, T. S. Jeong, M. S. Han and J. H. Kim, *J. Cryst.Growth*, 2004, 261, 526-532.

31. P. M. Chassaing, F. Demangeot, V. Paillard, A. Zwick, N. Combe, M. Kahn, A. Maisonnat, B. Chaudret, *Appl. Phys. Lett.*, 2007, 91, 053108-05310.

32. R. Bhargava, P. K. Sharma, S. Kumar, A. C. Pandey and, N. Kumar, *J. Raman Spectrosc.*, 2011, 42, 1802-1807.

33. B. C. Cheng, Y. H. Xiao, G. S. Wu, L. D. Zhang, *Appl. Phys. Lett.*, 2004, 84, 416-418.

34. G. Kortum, *Reflectance Spectroscopy, Springer-Verlag, New York Inc.*, 1969.

35. G. Cao, L. K. Rabenberg, C. M. Nunn, T. E. Mallouk, *Chem. Mater.*, 1991, 3, 149-156.

36. Y. S. Park, C. W. Litton, T. C. Collins, D. C. Reynolds, *Phys. Rev.*, 1966, 143, 512-519.

37. X. Y. Xu, C. B. Cao, *J. Alloys Compd.*, 2010, 501, 265-268.

38. Y. Kim, W. Lee, D. R. Jung, J. Kim, S. Nam, H. Kim, B. Park, *Appl. Phys. Lett.*, 2010, 96, 171902.

39. A. Popa, M. Lisca, V. Stancu, M. Bueda, E. Penita and T. Botila, *J. Optoelectron. Adv. Mater.*, 2006, 8, 43-45.

40. M. Ivill, S. J. Pearton, S. Rawal, L. Leu, P. Sadik, R. Das, A. F. Hebard, M. Chisholm, J. D. Budai, D. P. Norton, *New. J. Phys.*, 2008, 10, 065002.

41. H. Singh, A. K. Sinha, M. N. Singh, P. Tiwari, D. M. Phase, S. K. Deb, *J. Phys. Chem. Solids*, 2014, 75, 397–402.

42. A. C.Tuan, J. D. Bryan, A. B. Pakhomov, V. Shutthanandan, S. Thevuthasan, D. E. McCready, D. Gaspar, M. H. Engelhard, J. W. Rogers, K. Krishnan, D. R. Gamelin, S. A. Chambers, *Phys. Rev. B*, 2004, 70, 054424.

43. D. C. Frost, C. A. McDowell, I. S. Woolsey, *Mol. Phys.*, 1974, 27, 1473-1489.

44. T. Szore¨ ´nyi, L. D. Laude, I. Berto´ti, Z. Ka´ntor, Z. Geretovszk, *J. Appl. Phys.*,1995, 78 6211-6219.

45. J. C. C. Fan and J. B. Goodenough, *J. Appl. Phys.*, 1977, 48, 3524-3531.

46. P. F. Cai, J. B. You, X. W. Zhang, J. J. Dong, X. L. Yang, Z. G. Yin and N. F. Chen, *J. Appl. Phys.*, 2009, 105, 08371.

47. H. T. Ren, G. Xiang, G. X. Gu, X. Zhang, *Mater. Lett*, 2014, 122, 256-260.

48. Z. Zhang, D. C. Look, R.Schifano, K. M. Johansen, B. G. Svenssonand, L . J. Brillson, *J. Phys. D: Appl. Phys.*, 2013, 46, 055107.

49. J. H. Park, S. H. Lee, B. S. Kim, W. K. Kim, Y. C. Cho, M. W. Oh, C. R. Choand, S. Y. Jeong, *Appl. Phys. Lett.*, 2014, 104, 052412.

50. M. R. Hoffmann, S. T. Martin, W. Y. Choi, D. W. Bahnemann, *Chem. Rev.*, 1995, 95, 69–96.

51. F. Xu, Y. T. Shen, L. T. Sun, H. B. Zeng and Y. N. Lu, *Nanoscale*, 2011, 3, 5020-5025.

52. Moon-Deock. Kim, Jae-Eung. Oh, Song-Gang. Kim, W. C. Yang, *Solid State Commun*, 2011, 151, 768–770.

53. T. Watanabe, T. Takirawa and K. Honda, *J. Phys. Chem.*,1997, 81,1845-1851.

54. I. Izumi, W. W. Dunn, K. O. Wilbourn, F. R. F. Fan and A. J. Bard, *J. Phys. Chem.*, 1980, 84, 3207–3210.

55. R. W. Matthews, *J. Catal.*, 1986, 97, 565–568.

56. Q. Zhu, Y. Peng, L. Lin, C. M. Fan, G. Q. Gao, R. X. Wang and A. W. Xu, *J. Mater. Chem. A*, 2014, 2, 4429–4437.

Figure captions:

Fig. 1 (a) XRD patterns of ZnCoO, ZnCoO-Vac, ZnCoO-H and ZnCoO-Vac-H nanoparticles, (b) the expanded view of XRD patterns.

Fig. 2 TEM image of ZnCoO nanoparticles.

Fig. 3 The Raman spectra of ZnCoO, ZnCoO-Vac, ZnCoO-H and ZnCoO-Vac-H nanoparticles.

Fig. 4 (a) The UV-Vis diffuse reflectance spectra and (b) bandgap of pure ZnO, ZnCoO, ZnCoO-Vac, ZnCoO-H and ZnCoO-Vac-H nanoparticles

Fig. 5 XPS spectra of (a) Co 2*p* (b) O 1*s* for ZnCoO, ZnCoO-Vac, ZnCoO-H and ZnCoO-Vac-H nanoparticles.

Fig. 6 *M-H* curves of ZnCoO, ZnCoO-Vac, ZnCoO-H and ZnCoO-Vac-H nanoparticles. Inset is the expanded *M-H* curves of ZnCoO, ZnCoO-Vac nanoparticles.

Fig. 7 Photodegradation of RhB using ZnCoO, ZnCoO-Vac, ZnCoO-H and ZnCoO-Vac-H nanoparticles under the visible irradiation. Insets (Right) are the UV–vis absorption variations of RhB by ZnCoO-Vac-H, (Left) shows the photographs of RhB degradated by ZnCoO-Vac-H with time 0, 120, 240 min and magnetic recovery of the photocatalyst particles.

Fig. 8 Schematic diagram of the oxygen vacancies-related photocatalytic mechanism.

Table 1

The lattice parameters, crystallite sizes, band gap and the area ratio of the two O1s components O_b to O_a for ZnCoO nanoparticles annealed under different conditions.

Sample	a=b (Å)	c (Å)	Crystalline size (nm)	E_g(eV)	O_b/O_a
ZnCoO	3.2672	5.2306	31	2.58	0.270
ZnCoO-Vac	3.2728	5.2360	30	2.60	0.561
ZnCoO-H	3.2718	5.2364	35	2.54	0.339
ZnCoO-Vac-H	3.2722	5.2378	32	2.56	0.532

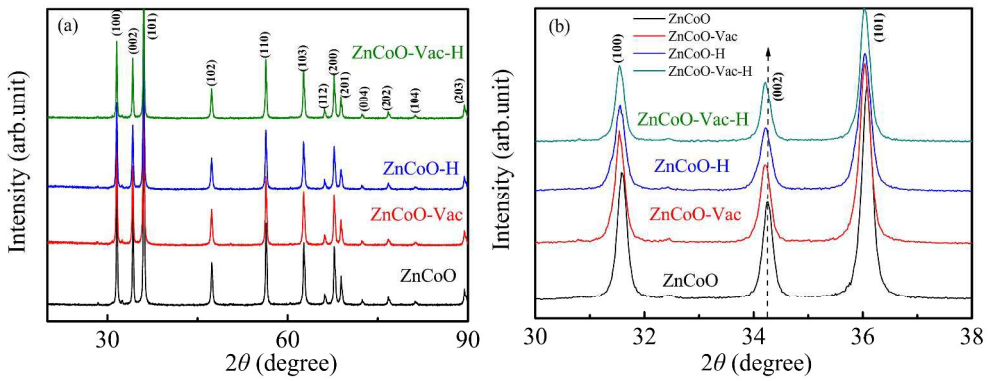

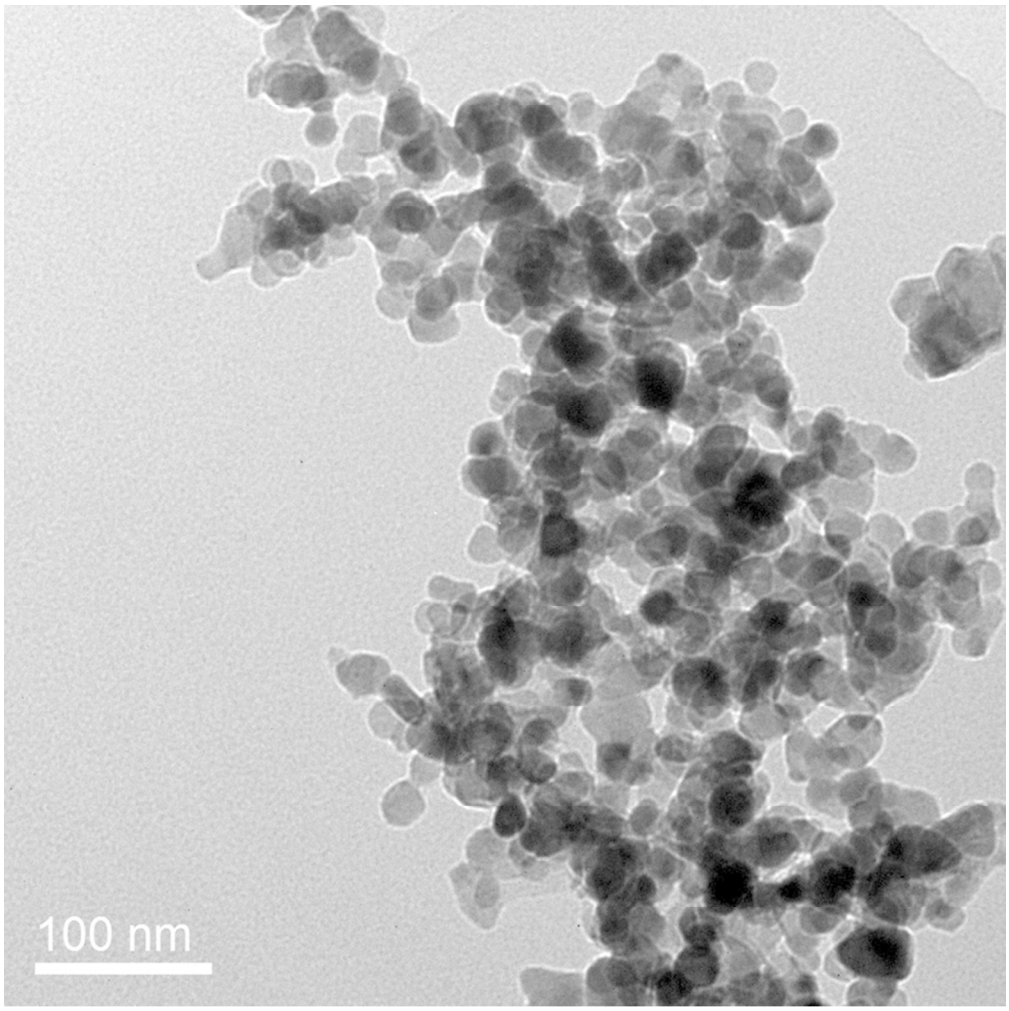

80x80mm (300 x 300 DPI)